

Image Denoising and Compression Based on Slant Haar Type Orthogonal Transforms

Xiuqiao Xiang¹, Baochang Shi^{2,*}, Jianga Shang¹, Linqun Yang¹, Yuhong Jiang¹

¹School of Computer Science, China University of Geosciences, Wuhan 430078, Hubei, China.

²School of Mathematics and Statistics, Huazhong University of Science and Technology, Wuhan 430074, Hubei, China.

How to cite this paper: Xiuqiao Xiang, Baochang Shi, Jianga Shang, Linqun Yang, Yuhong Jiang. (2026) Image Denoising and Compression Based on Slant Haar Type Orthogonal Transforms. *Journal of Applied Mathematics and Computation*, 10(1), 21-33.

DOI: 10.26855/jamc.2026.03.003

Received: January 15, 2026

Accepted: February 11, 2026

Published: March 9, 2026

***Corresponding author:** Baochang Shi, School of Mathematics and Statistics, Huazhong University of Science and Technology, Wuhan 430074, Hubei, China.

Abstract

The orthogonal transforms play a key role in signal processing, image processing, information security, etc. Despite their flexible generation and potential of the parameterized Slant Haar Type Orthogonal Transforms (SHTOT), SHTOT have received limited attention in the literature. In this work, we first investigate the recursive generation of Haar type orthogonal matrix (HTOT), slant matrix, and slant Haar matrix from the viewpoint of matrix. Then, the recursive generation and fast algorithms of SHTOT are achieved by combining HTOT and the slant matrix. In the end, we introduce SHTOT to the denoising and compression of standard images, and carry out a series of numerical experiments. The research in this paper demonstrates that different SHTOT with fast algorithms may be generated conveniently in the same program code only by varying any one value of two parameters. Moreover, SHTOT, particularly with parameters ($s=2$, $r=1$), achieves compression and denoising performance competitive with or superior to Haar, Walsh, slant transforms, discrete cosine transform, and discrete wavelet transform in several test cases, while offering a unified generation framework.

Keywords

Slant Haar type orthogonal transform; fast algorithm; image compression; image denoising; signal processing

1. Introduction

The time domain signals may be converted to the frequency domain form for the further analysis and utilization by the orthogonal transforms, which are widely applied in the signal processing, image processing, digital communication, information security, etc [1, 2]. It is well known that frequently used orthogonal transforms comprise Fast Fourier transform (FFT), Discrete Cosine Transform (DCT), Discrete Wavelet Transform (DWT), Fast Walsh transform (FWT), etc [3, 4], among which Discrete Fourier transform (DFT) may change a finite length signal to the superposition of sine waves with different frequencies. If the expanded function is real and even, then its Fourier series expansion only contains the cosine term. Namely, DCT is actually a special form of DFT. To significantly reduce the computational complexity, fast algorithm for DFT was provided in the form of FFT [5, 6]. Since the application of DFT, FFT and DCT is limited because of their global bases, wavelet transform containing short attenuated wavelet basis was generated, which may analyze the signals effectively due to its local localization ability and multi-resolution characteristics [7, 8].

From wavelet analysis [9], Haar function is the simplest wavelet, rows of Haar orthogonal matrix denote Haar wavelets at different scales and times. Walsh function corresponds to Haar wavelet packet, and rows of Walsh orthogonal matrix represent different Walsh functions, which means that the signals are fully decomposed and analyzed

Thus, we may get different SHTOM by varying the slant mutation parameters a_k, b_k arbitrarily under the constraint (4).

Remark 4: Although Walsh matrix and slant matrix exist four orders that correspond to different arrangements of matrix rows [14, 18], in this paper, we only discuss M order matrix, which has an in-place fast algorithm suitable for real-time applications.

2.1 Recursive generation of Haar type orthogonal matrix

Wavelet analysis is an excellent information processing tool [16, 17]. As the simplest wavelet, Haar wavelet doesn't participate in the further decomposition of the high-frequency parts, as shown in Fig. 1c. Walsh wavelet is Haar wavelet packet, that is, both the low frequency and high frequency parts execute thorough decomposition, as illustrated in Fig. 1a. Accordingly, Haar type orthogonal matrices (HTOM) include Haar, Walsh and other wavelet matrices in between, the high frequency part is decomposed partly. For example, Her wavelet in HTOM is exhibited in Fig. 1b.

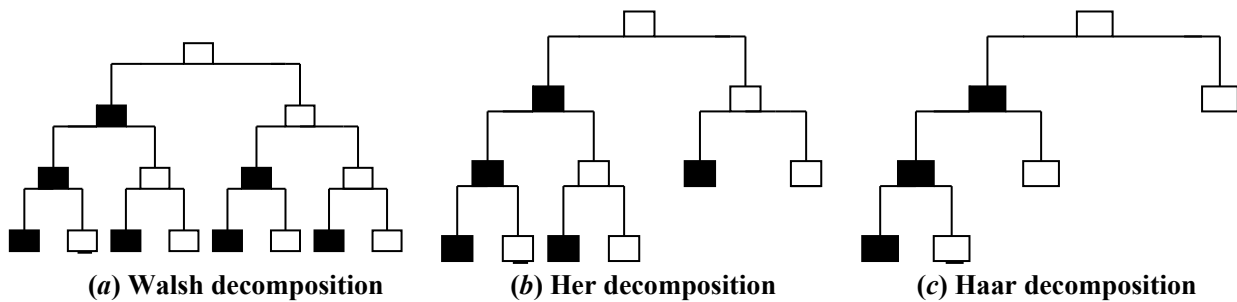


Figure 1. Decomposition flow of the 8th-order Walsh Wavelet packet.

In Fig. 1, the 8th-order Walsh, Haar, Her wavelets are decomposed recursively three times, among which the black boxes correspond to the low-frequency part, while the white boxes denote the high-frequency part.

In the past, HTOMs were generated recursively, and fast algorithms were provided correspondingly. Limited by space, we won't go into detail here. Interested readers, please check Refs. [12, 13].

2.2 Recursive generation of slant matrix and slant Haar matrix

From Ref. [14], the Walsh matrix may change to a slant matrix by introducing a slant mutation operation in the form of a slant base vector. Generally speaking, a higher-order slant matrix S_N can be recursively generated from lower order slant matrix, i.e.

$$\begin{aligned}
 S_N &= X_N F_N (I_2 \otimes S_{N/2}) = X_N F_N (I_2 \otimes X_{N/2} F_{N/2} (I_2 \otimes S_{N/4})) = \dots \\
 &= X_N F_N (I_2 \otimes X_{N/2} F_{N/2}) \dots (I_{N/4} \otimes X_4 F_4) (I_{N/2} \otimes H_2)
 \end{aligned} \tag{5}$$

According to Ref. [18], a Haar matrix may become a slant Haar matrix by exerting a slant mutation operation. Namely, the N order slant Haar matrix may be produced recursively by the copy and mutation of a low-order slant Haar matrix, i.e.

$$\begin{aligned}
 P_N &= X_N H_N (I_2 \otimes P_{N/2}) = X_N H_N (I_2 \otimes X_{N/2} H_{N/2} (I_4 \otimes P_{N/4})) = \dots \\
 &= X_N H_N (I_2 \otimes X_{N/2} H_{N/2}) \dots (I_{N/4} \otimes X_4 H_4) (I_{N/2} \otimes H_2)
 \end{aligned} \tag{6}$$

Note that X_k, H_k, F_k in Eqs. (5), (6) are defined in Eq. (2).

2.3 Recursive generation and fast algorithm of SHTOT

From subsection 2.1, the Haar matrix and the Walsh matrix are both special cases of Haar type orthogonal matrices (HTOM). From subsection 2.2, the slant Haar matrix, slant matrix, are generated by introducing the slant mutation

operation on Haar matrix, Walsh matrix, respectively. Inspired by this, HTOM may become slant Haar type orthogonal matrices (SHTOM) as follows.

Let $K = 2^s$, $R = 2^{s-r}$, $N = KR^m$, both s and r ($s > 1, 0 < r < s$) are integers, $m=0, 1, 2, \dots$, then the N order SHTOM denoted as SH_N can be generated recursively by attaching a slant mutation operation.

$$SH_N = SH_{KR^m} = X_{KR^m} T_{KR^m} (I_R \otimes SH_{KR^{m-1}}) \tag{7}$$

$$= X_{KR^m} T_{KR^m} (I_R \otimes X_{KR^{m-1}} T_{KR^{m-1}}) (I_{R^2} \otimes SH_{KR^{m-2}}) \tag{8}$$

$$= \left[\prod_{i=0}^{m-1} (I_{R^i} \otimes X_{KR^{m-i}}) (I_{R^i} \otimes T_{KR^{m-i}}) \right] (I_{R^m} \otimes M_K) \tag{9}$$

where $T_{KR^{m-i}}$ represents the KR^{m-i} order Haar type mutation matrix, which has the following decomposition form or fast algorithm.

$$T_{KR^{m-i}}(s, r) = T_{KR^{m-i}}^{(s-1)} (I_2 \otimes T_{KR^{m-i}}^{(s-2)}) \cdots (I_{2^{s-r-1}} \otimes T_{2KR^{s-i-1}}^{(r)}), \tag{10}$$

$$m=1, 2, \dots, \quad i=0, 1, 2, \dots, m-1$$

$T_{KR^{m-i}}^{(s-j-1)}$ indicates that the $KR^{m-i} 2^{-j}$ order identity matrix $I_{KR^{m-i} 2^{-j}}$ is inserted evenly by the 2^{s-j} order matrix $F_{2^{s-j}}$, $F_{2^{s-j}}$ is defined in Eq. (2). Thus,

$$T_{KR^{m-i} 2^{-j}}^{(s-j-1)} = \begin{pmatrix} A & C & \\ & A & D \\ C & & B \\ & C & A \end{pmatrix}, \quad A = \text{diag}\{I_{R^{m-i}}, I_{R^{m-i}}, \dots, I_{R^{m-i}}\} \tag{11}$$

$$B = \text{diag}\{B_{R^{m-i}}, B_{R^{m-i}}, \dots, B_{R^{m-i}}\}, \quad B_{R^{m-i}} = \text{diag}\{-1, I_{R^{m-i-1}}\},$$

$$C = \text{diag}\{C_{R^{m-i}}, C_{R^{m-i}}, \dots, C_{R^{m-i}}\}, \quad C_{R^{m-i}} = \text{diag}\{1, 0_{R^{m-i-1}}\},$$

$$D = \text{diag}\{D_{R^{m-i}}, D_{R^{m-i}}, \dots, D_{R^{m-i}}\}, \quad D_{R^{m-i}} = \text{diag}\{-1, 0_{R^{m-i-1}}\}, \quad j = 0, 1, 2, \dots, s-r-2, s-r-1.$$

$X_{KR^{m-i}}$ in Eqs. (7-10) denotes the KR^{m-i} order slant mutation matrix defined in Eq. (2). The K order Walsh matrix M_K in Eq. (9) has the following fast algorithm [12].

$$M_N = \begin{pmatrix} M_{N/2} & \hat{M}_{N/2} \\ M_{N/2} & -\hat{M}_{N/2} \end{pmatrix} = \begin{pmatrix} I_{N/2} & \hat{I}_{N/2} \\ I_{N/2} & -\hat{I}_{N/2} \end{pmatrix} \begin{pmatrix} M_{N/2} & \\ & M_{N/2} \end{pmatrix} = F_N (I_2 \otimes M_{N/2}) \\ = F_N (I_2 \otimes F_{N/2}) (I_4 \otimes F_{N/4}) \cdots (I_{N/4} \otimes F_4) (I_{N/2} \otimes H_2) \tag{12}$$

where $I_{N/2}$ denotes the $N/2$ order identity matrix, $\hat{I}_N = \begin{pmatrix} I_{N/2} & \\ & -I_{N/2} \end{pmatrix}$, $\hat{M}_N = \hat{I}_N M_N$. F_K in Eq. (12) is defined in Eq. (2).

From Eqs. (7)-(12), SHTOM has an in-place fast algorithm very suitable for the real-time application. Without loss of generality, we take the 8th order Slant Haar Type Transform (SHTOT) for example, its algorithm flowchart is shown in Fig. 2.

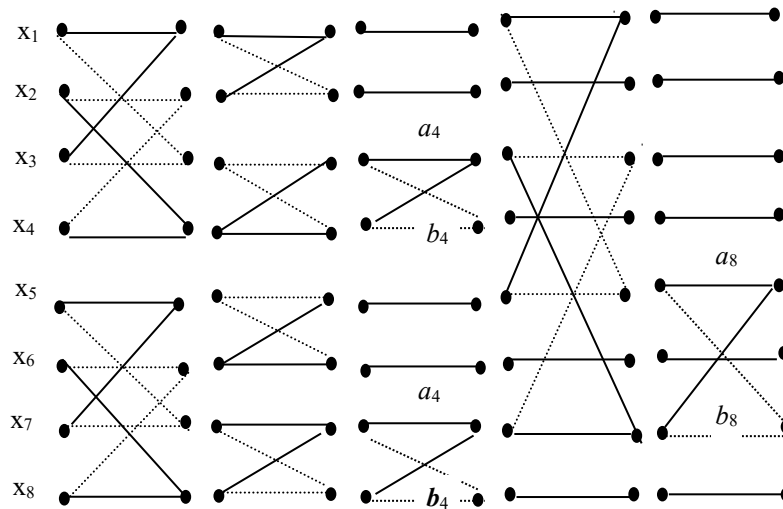


Figure 2. Algorithm flowchart of the 8th order SHTOT ($s=1, r=0$).

- (1) The parameters a_4, a_8, b_4, b_8 in Fig. 2 are computed by Eq. (3).
- (2) The butterfly diagram in Fig. 2 is explained in Fig. 3.

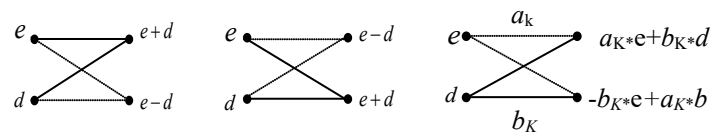


Figure 3. The meaning of the butterfly diagram.

Note that SHTOT utilized in this paper consist of slant Haar transform, slant transform and other orthogonal transforms intervenient former ones, such as slant her transform, slant Ter transforms, etc. SHTOT may possess the unique properties and potential usage in the image processing, as validated experimentally in next section. Moreover, different SHTOT can be generated conveniently in the same program code only by changing any one value of two parameters s and r . For instance, order $s=1, r=0$, slant Haar matrix is achieved, let $s=2, r=0$, slant Ter matrix is obtained. Additionally, SHTOT have the close relationship with other transforms, as demonstrated in Fig. 4.

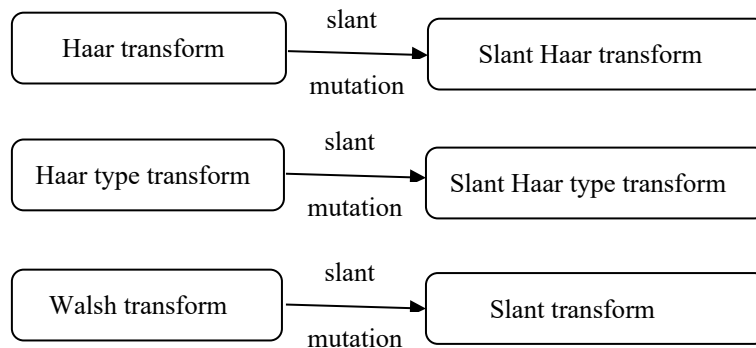


Figure 4. The relationship between different transforms.

3. Image experiment based on SHTOT

Slant Haar type orthogonal transforms (SHTOT) described in Ref. [18] have unique properties in some special fields. Nevertheless, SHTOT has attracted little attention from scholars' that they are rarely utilized in practice. For this reason, in this section, we introduce SHTOT to the denoising and compression of standard images—'Lena', 'Peppers', 'Baboon', 'Bridge', 'trees', and perform the comparison analysis with other transforms under the Matlab 6.1

environment. During the experiments, the Peak Signal-to-Noise Ratio (PSNR) and structural similarity index measurement (SSIM) are used for the evaluation of image quality. PSNR is defined in Eq. (13).

$$PSNR=10 \log\left(\frac{255 \times 255}{D^2}\right) \tag{13}$$

where $D^2 = \frac{\sum_{i=1}^m \sum_{j=1}^n (X(i, j) - Y(i, j))^2}{m \times n}$, X and Y denote the pixel matrix of $m \times n$ original image and decompressed image, respectively.

SSIM is defined by

$$SSIM(X, Y) = l(X, Y)^\alpha \cdot c(X, Y)^\beta \cdot s(X, Y)^\gamma \tag{14}$$

where $l(X, Y)$, $c(X, Y)$ and $s(X, Y)$ denote the brightness, contrast and structural differences of the images. Their definitions are described as follows:

$$l(X, Y) = \frac{2u_x u_y + C_1}{u_x^2 + u_y^2 + C_1} \tag{15}$$

$$c(X, Y) = \frac{2\sigma_x \sigma_y + C_2}{\sigma_x^2 + \sigma_y^2 + C_2} \tag{16}$$

$$s(X, Y) = \frac{2\sigma_{xy} + C_3}{\sigma_x \sigma_y + C_3} \tag{17}$$

Among them, u_x , u_y represent the average brightness of the original image X , decompressed image Y , respectively. σ_x , σ_y denote the brightness deviation of the image X , Y , respectively. σ_{xy} is the covariance between X and Y . Let C_1 , C_2 and C_3 be 1 to avoid zero denominator. The value of SSIM ranges from 0 to 1, and the closer SSIM is to 1, the smaller the difference between X and Y .

3.1 Image compression based on SHTOT

In this subsection, we perform the image compression experiment as follows. If the image is a X matrix with m rows and n columns, orthogonal transform is denoted as H , then the two-dimensional transform is expressed by

$$B = H * X * W \tag{18}$$

where W is the inverse of matrix H .

After the transform described in Eq. (18), we sort the transformed coefficients B from small to large, set 90% of the smaller transformed coefficient B to 0, and remain other larger transformed coefficients unchanged. In this way, matrix B change into matrix B_2 , the image data is compressed at a compression ratio $c=z/(m \times n)$, z denotes the number of transform coefficients set by zero. If we want to restore the original image X , we may apply the inverse transformation to matrix B_2 as follows

$$Y = W * B_2 * H \tag{19}$$

where Y is the recovered image similar to the original one.

According to the scheme described above, we perform the image compression by SHTOT. Meanwhile, we carry out a comparison experiment with other transforms. The compression images based on different transforms are shown in Figs. 5-6. Fig. 5(a) denotes the original ‘Lena’ image, Figs. 5(b), (c), (d), (e), (f), (g), (h), (l), (m), (n), and (p) represent the ‘Lena’ compression images based on Haar transform, Walsh transform, slant transform, DWT (take Slant-let wavelet for example), DCT, HTOT and SHTOT, respectively. Fig. 6(a) denotes the original ‘Peppers’ image, Figs. 6(b), (c), (d), (e), (f), (g), (h), (l) and (m) correspond to the ‘Peppers’ compression image based on Haar transform, Walsh transform, slant transform, DWT, DCT, HTOT and SHTOT, respectively.



Figure 5. Compression of 'Lena' image based on different transforms.



Figure 6. Compression of the 'pepper' image based on different transforms.

In addition, to evaluate the quality of compressed images quantitatively, PSNR and SSIM of the recovered image versus the compression ratio (c), images and transforms are summarized in Table 1.

Figs. 5, 6, and Table 1 demonstrate that SHTOT introduced in this paper still has good image quality even at a high compression ratio $c=98\%$. Moreover, SHTOT has compression effects varied with parameters s and r . Particularly, in many cases, Haar transform, DWT (Slant-let wavelet) and SHTOT with parameters $(s=1, r=0)$, $(s=2, r=0)$ or $(s=2, r=1)$ perform best in the image compression, compared with DCT, HTOT, Walsh, slant transform and SHTOT with other s, r values.

Table 1. Different image quality versus different transform and compression ratio (c)

Image Transform	Lena				Peppers			
	$c=90\%$		$c=98\%$		$c=90\%$		$c=98\%$	
	PSNR	SSIM	PSNR	SSIM	PSNR	SSIM	PSNR	SSIM
DCT	36.663	0.994	30.264	0.975	35.63	0.99	29.89	0.98
DWT(Slant-let)	38.18	0.996	30.99	0.979	37.03	0.99	31.07	0.98
Haar	38.031	0.996	30.608	0.977	36.73	0.994	30.17	0.98
Walsh	33.76	0.99	27.90	0.96	33.27	0.988	27.27	0.958
Slant	35.01	0.99	28.94	0.967	34.30	0.990	28.69	0.80
HTOT ($s=2, r=0$)	37.85	0.996	30.297	0.976	36.55	0.99	29.74	0.97
HTOT ($s=2, r=1$)	37.63	0.995	30.085	0.975	36.29	0.99	29.41	0.97
HTOT ($s=3, r=0$)	37.58	0.995	29.983	0.975	36.15	0.99	29.30	0.97
HTOT ($s=3, r=1$)	37.337	0.995	29.702	0.973	35.89	0.99	29.00	0.97
HTOT ($s=3, r=2$)	37.059	0.995	29.44	0.972	35.53	0.99	28.65	0.97
SHTOT ($s=1, r=0$)	38.234	0.996	30.822	0.978	36.733	0.995	30.29	0.976
SHTOT ($s=2, r=0$)	38.052	0.996	30.802	0.978	36.724	0.995	30.17	0.976
SHTOT ($s=2, r=1$)	38.216	0.996	31.204	0.98	36.865	0.995	30.64	0.978
SHTOT ($s=3, r=0$)	37.651	0.995	30.215	0.976	36.206	0.994	29.46	0.972
SHTOT ($s=3, r=1$)	37.551	0.995	30.217	0.976	36.103	0.994	29.51	0.973
SHTOT ($s=3, r=2$)	37.252	0.995	29.887	0.974	35.717	0.993	29.09	0.970

3.2 Image denoising based on SHTOT

In this subsection, we perform the image denoising experiments by the following scheme: add noise N to the original image X , $X_1 = X + N$, then transform X_1 by referring Eq. (18), get the matrix B_1 and set the smaller coefficients of matrix B_1 to zero 0. In this way, matrix B_1 change into matrix B_2 . Subsequently, take the verse transform of B_2 similar to Eq. (19). Finally, the denoising image Y_1 is obtained under the same conditions, as displayed in Figs. 7-9, image quality PSNR and SSIM versus different transform are listed in Table 2, in which *I, II, III* denote ‘Baboon+salt & pepper’, ‘Bridge+ gaussian’, ‘trees+ speckle’ cases, respectively.

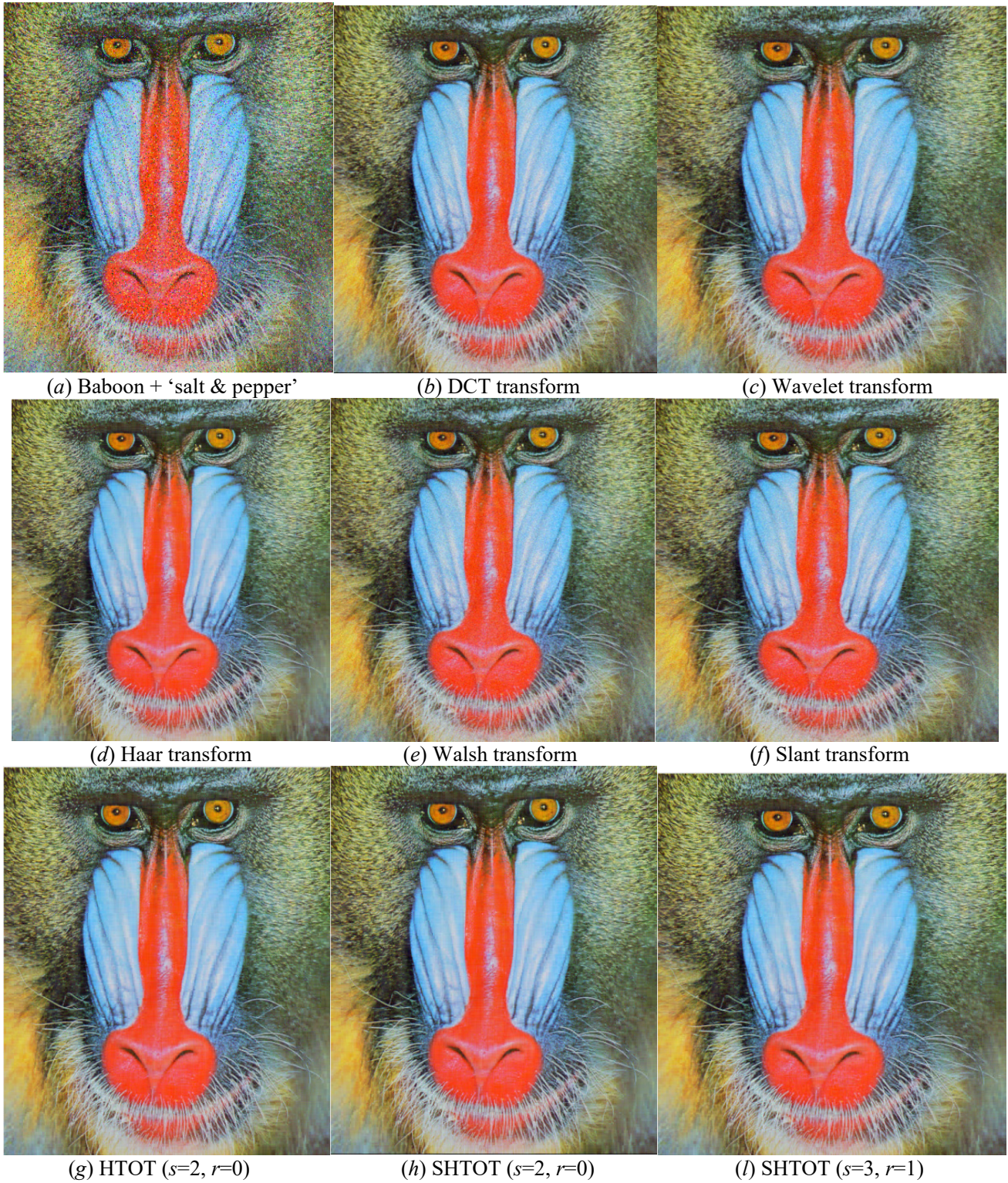


Figure 7. Denoising of 'Baboon+salt & pepper' image by different transforms.

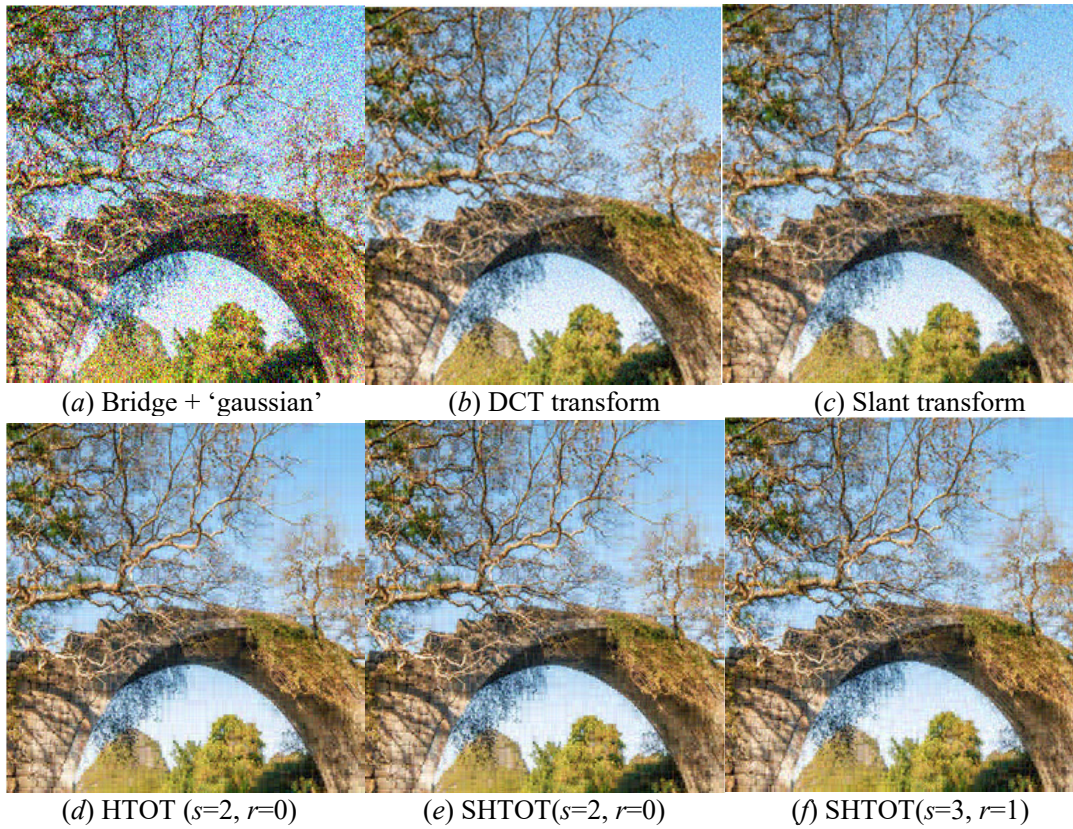


Figure 8. Denoising of 'Bridge + Gaussian' image by different transforms.

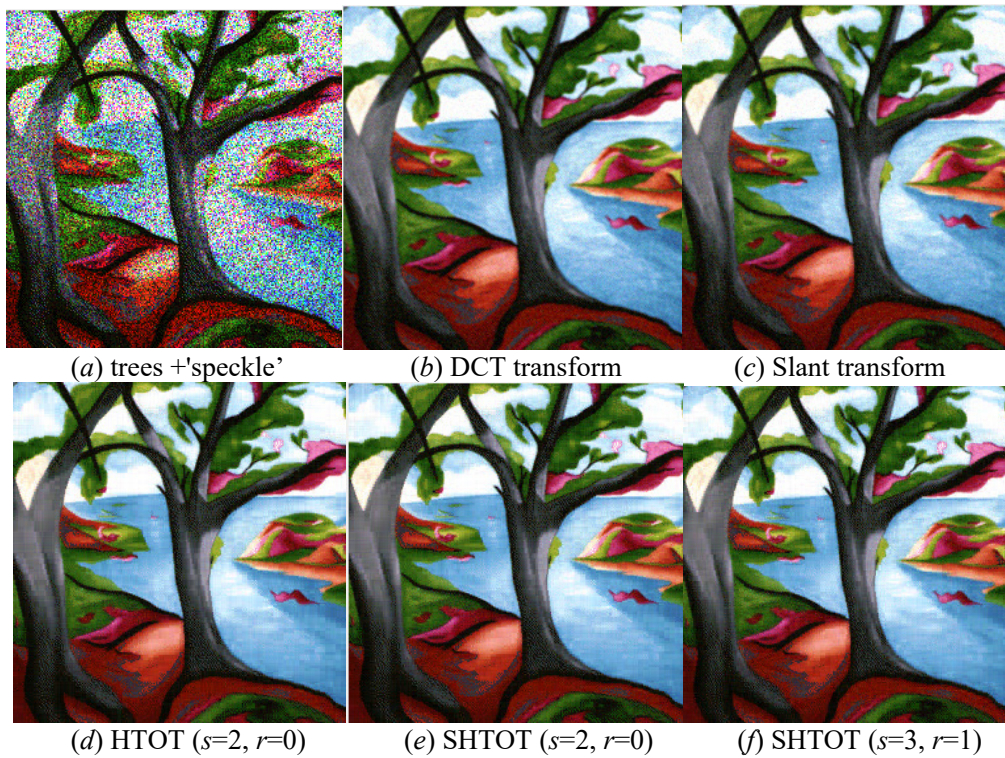


Figure 9. Denoising of 'trees + speckle' image by different transforms.

Table 2. Image denoising quality versus different transform

Noise Transform	I		II		III	
	PSNR	SSIM	PSNR	SSIM	PSNR	SSIM
DCT	26.93	0.923	24.371	0.903	27.898	0.913
DWT(Slantlet)	28.062	0.933	24.515	0.907	29.281	0.939
Haar	27.854	0.930	24.369	0.905	28.721	0.931
Walsh	25.726	0.900	23.291	0.878	26.134	0.881
Slant	25.997	0.905	23.538	0.884	26.962	0.897
HTOT ($s=2, r=0$)	27.803	0.929	24.325	0.904	28.424	0.928
HTOT ($s=2, r=1$)	27.71	0.929	24.218	0.902	28.098	0.924
HTOT ($s=3, r=0$)	27.750	0.930	24.176	0.901	28.015	0.922
HTOT ($s=3, r=1$)	27.666	0.929	24.136	0.900	27.765	0.919
HTOT ($s=3, r=2$)	27.548	0.928	24.025	0.898	27.403	0.912
SHTOT ($s=1, r=0$)	27.851	0.930	24.344	0.904	28.840	0.933
SHTOT ($s=2, r=0$)	27.899	0.931	24.318	0.904	28.663	0.931
SHTOT ($s=2, r=1$)	27.957	0.932	24.366	0.904	28.791	0.933
SHTOT ($s=3, r=0$)	27.781	0.931	24.211	0.902	28.001	0.922
SHTOT ($s=3, r=1$)	27.745	0.931	24.184	0.901	27.932	0.921
SHTOT ($s=3, r=2$)	27.627	0.929	24.077	0.899	27.499	0.914

Figs7-9 and Table 2 illustrate that PSNR and SSIM of the denoising image relate to the orthogonal transform utilized. Besides DWT (Slantlet) and Haar transform, SHTOT with parameters ($s=1, r=0$), ($s=2, r=0$), or ($s=2, r=1$) have better denoising effect compared with other transforms, such as DCT, Walsh, slant transform, HTOT, and SHTOT with other parameters (s, r) value. Except in special circumstances where $s=3, r=0$, SHTOT performs better than corresponding HTOT in most cases.

In addition, we compare the calculation time of different transforms under the same conditions, as presented in Table 3, where seconds is viewed as a unit of time.

From Table 3, we may draw a conclusion that the calculation time of SHTOT is slightly longer than that of other transforms. The important reason for this result is that the standard for programming is inconsistent; the time will be shorter if the program of SHTOT is further optimized.

Table 3. Calculation time versus orthogonal transform

Transform	DCT	DWT	Walsh	Slant	HTOT ($s=2, r=0$)	SHTOT ($s=2, r=0$)	SHTOT ($s=3, r=2$)	SHTOT ($s=3, r=0$)
Time (s)	0.229	0.214	0.236	0.217	0.4497	0.4518	0.3691	0.3364

4. Conclusion

In recent years, theory and application about orthogonal transforms have attracted widespread attention in the field of information science. Among the numerous orthogonal transforms, such as DCT, DWT, Haar, etc., slant Haar type orthogonal transforms (SHTOT) are recursively generated by combining Haar type orthogonal transforms (HTOT) and slant transform. Moreover, different SHTOT with fast algorithm are produced conveniently and flexibly in the same program code only by varying any one of two parameter value. Nevertheless, the excellent property of SHTOT has attracted little attention of scholars' that SHTOT are rarely utilized in practice. In this paper, we first investigate the recursive generation and fast algorithms of HTOT, slant transform, slant Haar transform and SHTOT using Walsh,

Haar copy, and slant mutation technique from a matrix standpoint. Then, we introduce SHTOT to the denoising and compression of standard images, and perform a series of comparison experiments, which demonstrate that the SHTOT family, particularly for specific parameter choices (e.g., $s=2$, $r=1$), can achieve image compression and denoising performance that is highly competitive with established transforms, such as the DWT, Haar, Walsh, and slant transform. The primary advantage of SHTOT lies not in universally superior performance, but in its parameterized framework that unifies several classical transforms and allows for tuning based on application needs.

Data availability

Data will be made available on request.

Funding

This work was supported by the National Natural Science Foundation of China [Grant number. 6120205].

References

- [1] Kozhan R, Vaktnäs M. Christoffel transform and multiple orthogonal polynomials. *J Comput Appl Math.* 2026;476:117121.
- [2] Monaim H, Faress M. General double-sided orthogonal split quadratic phase Clifford-Fourier transform. *J Math Anal Appl.* 2025;543(2):129009.
- [3] Jiang R, Qiao K, Liu C, Yuan W. A low-complexity expectation propagation symbol detector for DCT-OTFS systems. *Phys Commun.* 2026;74:102986.
- [4] Tan D, Yang D, Tan B, et al. AOT-PixelNet: Lightweight and interpretable detection of forged images via adaptive orthogonal transform. *Appl Soft Comput.* 2025;185:113873.
- [5] Elliott DF, Rao KR. *Fast transforms: algorithms, analyses, applications.* New York: Academic Press; 1982.
- [6] Xavier Chelliah AG. A normal I/O order optimized dual-mode pipelined FFT architecture for processing real-valued signals and complex-valued signals. *AEU-Int J Electron C.* 2023;170:154782.
- [7] Deng Y, Ding K, Ouyang C, Luo Y, et al. Wavelets and curvelets transform for image denoising to damage identification of thin plate. *Results Eng.* 2023;17:100837.
- [8] Chen H, Zhang J, Yu T, Zeng Y, Zeng H. RetinexWT: Retinex-based low-light enhancement method combining wavelet transform. *Digit Signal Process.* 2026;126:105947.
- [9] Zhang D, Ni W, Fu N, et al. Locally differentially private multi-dimensional data collection via Haar transform. *Comput Secur.* 2023;130:103291.
- [10] Xiang X, Zhou J, Li C, et al. Fault diagnosis based on Walsh transform and rough sets. *Mech Syst Signal Pr.* 2009;23(4):1313-26.
- [11] Xiang X, Shi B. Evolving generation and fast algorithms of Slant-let transform and Slantlet-Walsh transform. *Appl Math Comput.* 2015;269:731-43.
- [12] Xiang X, Zhou J, Yang J, et al. Mechanic signal analysis based on the Haar-type orthogonal matrix. *Expert Syst Appl.* 2009;36(6):9674-7.
- [13] Shi BC, Guo ZL, Wang NC. The evolving generation and fast algorithms of Haar-type transform. *Math Mag.* 1998;18:1-6. Chinese.
- [14] Shi BC, Wang NC. The evolving generation and fast algorithms of Slant transform. *Math Numer Sin.* 2000;22:437-48. Chinese.
- [15] Wang Z. New algorithm for the slant transform. *IEEE T Pattern Anal.* 1982;4(4):551-5.
- [16] Jia D, Liu L, Zhu L, et al. Adaptive embedding: A novel meaningful image encryption scheme based on parallel compressive sensing and slant transform. *Signal Process.* 2021;188:108220.
- [17] Rao KR, Kuo JGJ, Narasimhan MA. Slant-haar transform. *Int J Comput Math.* 1979;7(1):73-83.
- [18] Shi BC, Wang NC. The evolving generation and fast algorithms of slant Haar-type transform. *Math Numer Sin.* 2003;32:1-7. Chinese.